Strong-weak network anisotropy switching and hysteresis in three-dimensional granular materials

Xavier García and Ernesto Medina
Centro de Física, Instituto Venezolano de Investigaciones Científicas, IVIC, Apartado 21827, Caracas 1020 A, Venezuela
(Received 23 May 2008; published 26 August 2008)

We address hysteresis of three-dimensional polydisperse granular packs, comparing macro- and microscopic viewpoints, to reveal their elastic/inelastic mechanics and force network anisotropy. During the uniaxial loading-unloading cycle of an appropriately prepared pack, one can decompose the force network into weak and strong subnetworks. The first stages of loading exhibit arching, where all the fabric displays negative anisotropy. For later stages, the strong (weak) network shows positive (negative) anisotropy. On unloading, the force network progresses to a *fabric wide hydrostatic point*, where the anisotropies of the weak and strong subnetworks switch signs. During the loading stage, a Mohr circle analysis permits the identification of a well-defined macroscopic internal friction angle, whose value is larger than that of grain-grain interactions. To analyze unloading, a generalized local Coulomb-friction argument predicts a continuously changing friction angle, that vanishes at the hydrostatic point. A suggestive interplay between microscopic friction and fabric structure, at different loding stages, is proposed as the mechanism for the emergence of a macro internal friction angle.

DOI: 10.1103/PhysRevE.78.021305 PACS number(s): 45.70.−n, 83.80.Fg, 62.20.M−

I. INTRODUCTION

The behavior of granular materials under loading has been a subject of strong recent interest since it reveals many of the unique mechanical features of this phase of matter. Many of these features are inherited by granular rocks under uniaxial loading, and the anisotropic stresses developed under these conditions determine their mechanical strength and behavior under shear. The behavior of granular packs under cycles of compression is well known to exhibit hysteresis [1–4], manifested as different paths in the lateral to compressive stress curves as one increases and then decreases the applied load. While there has been a considerable number of theoretical and experimental work on loading of polydisperse grains [4–7], the behavior of the resulting pack when stress is lifted has received much less attention.

In the literature of soil mechanics the result of burdening sands uniaxially and then lifting the burden has been described as an *overconsolidated* state [8–11] as it is commonly termed. Depending on the origin of the granular pack, i.e., whether it originated from a process of deposition or was compactified from a random mixture, it must undergo a number of cycles before reaching a reproducible hysteresis cycle. The convergence to the limit cycle is of interest in itself [12], since the parameters that evolve to determine a unique mechanical behavior are unknown and generally correspond to those that minimize internal friction.

A phenomenological model for hysteresis in granular rocks has been developed in the context of Preisach-Mayergoyz (PM) models [13,14] where hysteretic mesoscopic units go a considerable way in explaining hysteresis and discrete memory effects [14]. Nevertheless, such models are only loosely based on the microscopic underpinnings such as the details of grain contacts. On the other hand, anisotropy induced by stress, either pure shear or isotropic stress to study filamentary force network characteristics has been addressed in a number of theoretical [15] and experimental [16] works. These works show how one can distinguish between shear and isotropic stresses in the network by way of the force distribution and correlations of tangential and normal forces.

In this paper we address hysteresis and anisotropy of a uniaxially loaded pile from both the macroscopic and the microscopic force fabric points of view. We show that unloading a granular material is starkly different from its loading counterpart and reveals features of recently developed scenarios of granular systems under loading in terms of a force network fabric [6,7]. We follow the anisotropic orientation of the force fabric as a function of loading and unloading and find, on the unloading path, a striking feature: *anisotropy switching*, a regime where the strong network [6] changes from the vertical to perpendicular while the uniaxial stress is still nonzero. After switching, the material preserves an intrinsic anisotropy even while completely unloaded, describing the overconsolidated state. The two regimes are separated by a global (isotropic strain) and local (isotropic fabric) *hydrostatic point*. During loading, on the other hand, the fabric reveals clear evidence of arching before a strong network positive anisotropy develops. The strong and weak networks respond very differently to increasing/decreasing stress.

Finally, we make contact with a well-known rock mechanics tool, the Mohr circle, in order to define a macroscopic friction angle. On loading one can compute a well-defined macro friction coefficient that is larger than that of the grain-grain interaction. This we discuss in terms of the average geometry of the stress planes given by the force fabric. On unloading, the macro internal friction seems to vary continuously and vanishes at the hydrostatic point.

II. GRANULAR MODEL

Very accurate representations of unconsolidated sands have been developed in three dimensions [5] that consider a

nonlinear Hertz-Mindlin model for the grain-grain interactions and also account for surface elasticity [17]. The predictions of the Hertz-Mindlin model are in close correspondence to experimental tests [12] of relatively homogeneous sand packs without cementation (see also Ref. [9]).

At the microscopic level, when two grains come into contact, they interact with a repulsive nonlinear viscoelastic force [5,12,17] $\mathbf{F}_c$ given by

$$\mathbf{F}_c = \{\sqrt{\xi_n R_f}(\kappa_n \xi_n - \gamma_n \dot{\xi}_n)\}\hat{\mathbf{n}} + \mathbf{F}_s, \tag{1}$$

where the first term, on the right-hand side, represents the force $\mathbf{F}_n$ normal to the contact area. For the labeled grains 1 and 2 with radii R_1, R_2 and positions $\mathbf{r}_1$, $\mathbf{r}_2$, $\xi_n = \max(0, R_1 + R_2 - |\mathbf{r}_2 - \mathbf{r}_1|)$ and $\hat{\mathbf{n}} = (\mathbf{r}_1 - \mathbf{r}_2)/|\mathbf{r}_1 - \mathbf{r}_2|$ is the unitary vector joining the grain centers. The normal stiffness of the contact, $\kappa_n = 4G/(1-\nu)$, where $G = 29$ GPa is the shear modulus and $\nu = 0.08$ is the Poisson coefficient, $R_f = (R_1 R_2)/(R_1 + R_2)$ is an effective radius and $\sqrt{\xi_n R_f}$ is the radius of the contact area. The second term in braces in Eq. (1) represents the the viscous forces for normal deformations, where γ_n is a damping constant set here to 2.3×10^{-6} gr/(cm s).

The shear force in Eq. (1)

$$\mathbf{F}_s = -\min(\sqrt{\xi_n R_f}(\kappa_s \vec{\xi}_s - \gamma_s \vec{\dot{\xi}}_s), \mu |F_n| \hat{s}) \tag{2}$$

depends on contact history and cannot be entirely determined by the position of grains. Such force is given by Eq. (2), where the tangential stiffness is $\kappa_s = 8G/(2-\nu)$ and μ represents the Coulomb friction coefficient here set to 0.3. The term $\gamma_s = 2.0 \times 10^{-6}$ gr/(cm s) is a damping coefficient and $\xi_s = \int_0^t \dot{\xi}_s(t')dt'$ is the tangential displacement that took place since the contact was first established. If $\vec{\dot{\xi}}$ is the relative velocity of the grain surfaces, $\vec{\dot{\xi}}_s = \vec{\dot{\xi}} - (\vec{\dot{\xi}} \cdot \hat{n})\hat{n}$, and $\hat{s} = \vec{\dot{\xi}}_s / |\vec{\dot{\xi}}_s|$. The vector $\vec{\xi}_s$ can be computed from the relative displacement vector $\mathbf{d}$ between the grains in contact as $\vec{\xi}_s = \mathbf{d} - (\mathbf{d} \cdot \hat{\mathbf{n}}_0)\hat{\mathbf{n}}_0$, with $\hat{\mathbf{n}}_0$ the normal of the contact when it is created. Whenever a contact is established for the first time, the viscoelastic part of Eq. (2) (left term) is activated and the grains feel a force opposing to the tangential displacement. When the threshold of Coulomb dry friction is exceeded, sliding occurs following the frictional term (right) in Eq. (2) and the elastic spring is broken. When the tangential velocity drops to zero or is inverted, the elastic spring is reactivated with zero elongation and the friction force is turned off.

The initial pack contructed following [18] models a high porosity $\phi = 41.2\%$ sand, where contacts involve marginal contact areas. The radius of each particle is extracted from a given grain size distribution. In our simulations, the radius R of each particle is selected with equal probability in the range 0.018–0.021 cm, modeling a well-sorted sand. Periodic boundary conditions are imposed on perpendicular directions to the uniaxial stress field to emulate an effectively larger system and the confinement in those directions. The size of the generated sample was $24 \times 24 \times 32$ in units of the maximum grain diameter. Following previous results [18], this volume is several times larger than the minimum homogenization volume for the porosity of a sample with the given grain size distribution. This homogenization volume is consistent with that reported in Ref. [19] for a granular medium, like the one considered here, where it lies between two and three times the typical particle diameter.

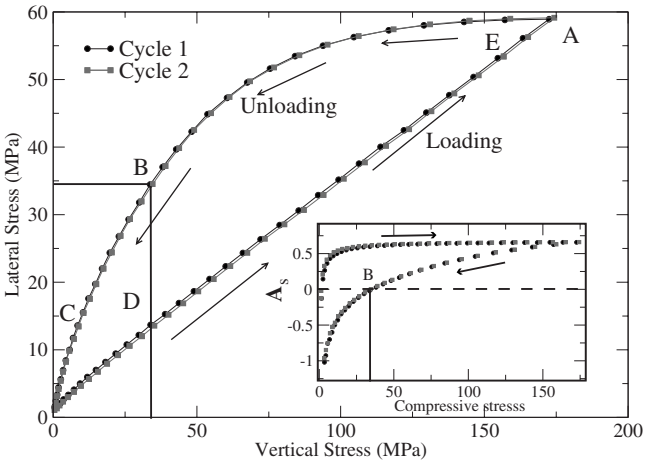

FIG. 1. Lateral stress as a function of the loading vertical stress. The loading-unloading process follows the arrows shown. Two loading/unloading cycles are shown so that it is clear that one has reached a limiting behavior. The inset depicts both cycles from the point of view of the macroscopic anisotropy. Point B indicates the hydrostatic point where anisotropy changes sign.

The sample is compressed isotropically without friction to produce a dense pack of porosity ~36% and mean coordination number ~6. This is done isotropically and without friction in order to avoid ingraining anisotropies in the granular pack using the following procedure: The first step involves positioning the grain on a grid so that they do not overlap. The typical interparticle spacing in this first step is two diameters of the largest particle radius. Then the particle positions are perturbed in their original positions 1% of the largest radius in a random direction and given an initial velocity. The ensemble of particles is then evolved long enough for the grains to collide and disorder their positions with no gravity considered. It is only then that the walls close in to compact the granular gas. Next, friction is turned on and several compaction-decompaction cycles are simulated following Ref. [12], until the stress-strain curve for two consecutive cycles show negligible differences. Note that one cannot get rid of hysteresis by cycling further, due to tangential friction in contrast to previous models [5] dominated by grain rearrangements.

III. ANISOTROPY AND HYSTERESIS UNDER UNIAXIAL STRESS: THE FABRIC

Two consecutive cycles of loading/unloading are shown in Fig. 1, where the laterally induced stress $\sigma_l = (\sigma_1 + \sigma_2)/2$ is shown as a function of the compressive stress $\sigma_c = \sigma_3$. The uniaxial stress is increased from zero to close to 175 MPa, and then reduced back to zero. This is done in appropriate small steps so as to allow for sufficient relaxation. During the first steps, the lateral stress grows at a relatively low rate, thus the macroscopic stress anisotropy $A_c = (\sigma_c - \sigma_l)/\sigma_c$

grows sharply (see inset). As the sample is compacted further, the rate of increase of the lateral stress grows until it approximately equals the compressive stress and a quasilinear behavior follows. This behavior is observed from the point of view of the stress anisotropy (see inset) where after around 50 MPa, the anisotropy saturates to a maximum value.

When the maximum loading is achieved (point A) and decompaction begins, the lateral stress reduces at a slower rate than the compressive stress and thus A_c slowly decreases. This entails an almost flat response to a rapid decrease of the compressive stress. The stresses evolve in such a way that their magnitudes become equal (at 35 MPa), a point at which the stress field is macroscopically hydrostatic (point B). Below this point, the lateral stress is greater than the compressive stress and the *anisotropy becomes negative* [10], as can be clearly seen in the inset of Fig. 1. The hydrostatic point is then the *switching point* for the principal stresses of the granular pile. Below this point (C) the lateral stress decays, overtaking the rate at which the compressive stress diminishes, until both join close to zero stress. Thus there is a maximum negative anisotropy before a complete collapse of the macroscopic anisotropy. As we will see below, the inhomogeneous nature of the force network, underlying the described behavior, can still possess anisotropy that is not evident from macroscopic measurements. The force network analysis proposed by Radjai *et al.* [6] has become a very useful tool to understand the relation between the macroscopic stress state and the local geometry of contacts in granular packs. Their proposal was to follow different tensor quantities in the network measuring the geometric orientation of the contacts, and their strengths as a function of the force fraction carried by them referred to the mean. Here we compute the fabric tensor generalized to three dimensions in order to determine the eigendirections in the granular pack as a function of the applied stress. The fabric tensor [6,20] is defined as

$$T_{ij}(\xi) = \langle n_i n_j \rangle = \frac{1}{N_\xi} \sum_{k}^{(\xi)} n_i^k n_j^k, \tag{3}$$

where ξ denotes the subset of contacts that carry forces smaller than $\xi F/\langle F \rangle$. The terms n_i denote the ith component of the unitary vector $\hat{n}^k$ pointing along the line that joins the center of the two particles at contact k. N_ξ is the total number of bonds belonging to the interval $(0,\xi)$. The eigenvalues of T_{ij}, denoted by ϕ_i $(i=1,2,3)$, are computed for several stress states. Due to uniaxial compaction $\phi_1 \sim \phi_2$ while ϕ_3 is along the uniaxial stress direction. One can then compute the anisotropy index $A_c(\xi)=(\phi_3 - 1/2(\phi_1+\phi_2))$.

Figure 2 depicts the fraction of bonds carrying forces below ξ and the anisotropy corresponding to the same fraction at the midpoint of the loading stage. It reveals the essential features described in Refs. [6,7] where more than 80% of the contacts carry a negative anisotropy (directed preferentially perpendicular to the loading direction) while about 10% of the bonds carry a positive anisotropy. As the load must be supported, the 10% above must carry the burden, and constitute, albeit few, the strongest bonds in the network. Other

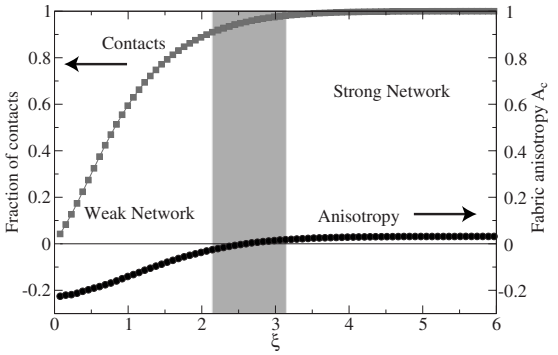

FIG. 2. Fraction of bonds carrying forces ξ, normalized by the average force $\langle F \rangle$ and the anisotropy carried by such a subset. The gray area in the plot highlights the possible transition region between the weak and strong networks in the vicinity of the anisotropy sign change. Less than 10% of the contacts (strong network) carry a positive anisotropy.

than the change in sign of the anisotropy, there is no clear line separating the strong and weak networks (see Fig. 2) but the concept of two networks is clearly meaningful.

The previous concept becomes more telling when we describe the evolution of the fabric tensor as a function of the loading/unloading process. Figure 3, top panel, shows the unloading stage where the small force network carries a strong negative anisotropy while the strong network a positive one at full loading. The figure shows that the anisotropy of relatively weak contacts reduces to one-fifth of its maximum value while the strong network changes by less than a half of its original value. Meanwhile, the global anisotropy decreases negligibly in the same interval (see Fig. 1 inset). These results evidence that the preferential orientation of the weak contacts change at a faster rate than those of the strong network. As decompaction progresses, the orientation of the contacts is randomized $[A_c(\xi) \sim 0]$ for all ξ. This corresponds to a hydrostatic stress state, and according to the fabric anisotropy, it is a global phenomenon of the network and not a result of compensating anisotropies of subset networks. Further decompaction leads to a preferential orientation of the strong network along the lateral direction while the weak contacts tend to align along the vertical direction. This is seen in Fig. 3, where $A_c(\xi)$ decreases monotonically and becomes negative beyond $\xi \sim 2$. At the end of decompaction, the orientation of the weak contacts and strong contacts is *switched*.

When the sample is reloaded after unloading, as shown in Fig. 3, bottom panel, the starting configuration involves a preferred orientation of weak contacts in the vertical direction, and in the lateral directions for the strong contacts. As compaction progresses, a dramatic change in the preferred orientation is observed, and the weak contacts preferentially align with the lateral direction along with the strong contacts. Surprisingly, all the fabric anisotropy is negative while there is a nonzero uniaxial stress. This is the clearest signal of the *arching* structure of the pile where all forces are directed to the sides. When sufficient loading is added, a strong network develops carrying a positive anisotropy, while the weak network develops a relatively stronger negative anisotropy.

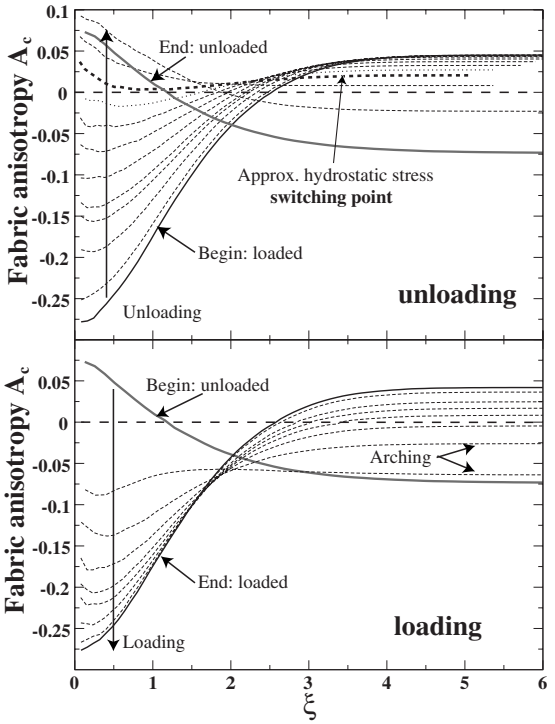

FIG. 3. Evolution of the geometric anisotropy A_c during loading and unloading of the granular pile. Top panel: Unloading stage shows the evolution of the fabric anisotropy as one samples larger values ξ in the network. The bold dashed line shows the point of hydrostatic local stresses and also the network switching point. Bottom panel: Loading stage shows the evolution of the fabric anisotropy. The two indicated dashed lines depict a situation where the fabric displays a negative anisotropy for all ξ, an evidence of arching in the beginning of all loading cycles.

IV. MOHR'S CIRCLE AND INTERNAL FRICTION

An insightful macroscopic description of the loading/unloading process can be obtained from the Mohr circle of the granular pile. In this representation, the normal and shear components applied instantaneously to every plane in the material as a result of the uniaxial stress are described. Unlike most laboratory tests, the lateral stress is not fixed, so the dynamics of both principal stresses are monitored simultaneously. A series of Mohr circles are shown in Fig. 4; the dashed line circles represent the loading series, while the solid line circles portray the unloading series. The intersection of the circles with the horizontal axis represent the main stress eigenvalues, the largest σ_3 in the uniaxial direction, and the smallest $(\sigma_1+\sigma_2)/2$. Figure 4 depicts two angles: ϕ is the internal effective friction angle as derived from the tangent to the Mohr circles when anisotropy has saturated. On the other hand β is the angle between a particular plane and the uniaxial strain direction. There one would see the combination $\tau-\sigma$, where τ is the tangential stress and σ is the normal stress applied to that plane.

The circles readily describe the evolution of macro anisotropy: When loading, beyond a small uniaxial stress, the anisotropy is a constant (see inset of Fig. 1), so a linear increase of the circle radii ensues (stresses in both directions increase at the same rate). The unloading follows a completely different path: The σ_3 decreases more rapidly than the lateral stress, which tends to accumulate the lower end of the circles close to 50 MPa. When the main stress reduces to 50 MPa, the lateral stresses begin to relax at a faster rate and one approaches the hydrostatic point where $\sigma_3=(\sigma_1+\sigma_2)/2$. As shown for the fabric, the pile has hydrostatic character both microscopically and macroscopically. This stress switching point gives way to inverted Mohr circles that first grow in the opposite direction [with $\sigma_3<(\sigma_1+\sigma_2)/2$] before decreasing to zero as uniaxial stress dissappears. It is clear that the local anisotropy, a remnant in the fabric exhibited in Fig. 3, is not manifest in the global stress anisotropy as shown by the Mohr circles.

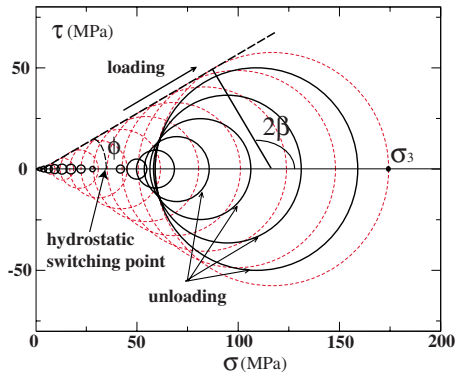

FIG. 4. (Color online) The Mohr circles as a function of the loading (dashed line circles) and unloading (continuous line circles). The vertical axis is the tangential stress applied to a plane at an angle of 2β from the main principal axis σ_3. σ_1 is drawn as the lateral principal value at the opposite intersection of the circle with the horizontal axis. As loading increases for $\mu=0.3$, both σ_1 and σ_3 increase, generating a new circle. All loading circles share the same tangent beyond a small loading, while unloading is highly nontrivial.

When load is applied, the granular pile deforms, accumulating elastic energy and dissipating energy by sliding contacts. The friction coefficient dependence of anisotropy and how it is related to macroscopic properties is then a revealing feature of the emergent mechanical behavior of the granular pile. In Fig. 5 we show the macroscopic saturation anisotropy (see inset of Fig. 1) as a function of the microscopic

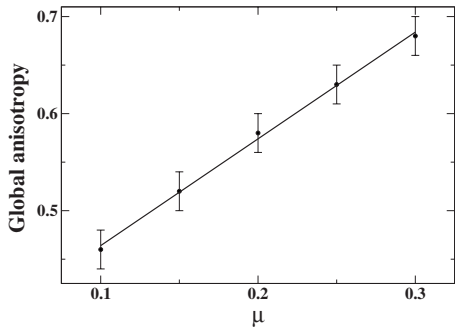

FIG. 5. The global anisotropy $(\sigma_3-\sigma_1)/\sigma_3$ as a function of the microscopic (grain-grain) friction coefficient for loading. As discussed in the text the granular friction coefficient is smaller than the emergent one as derived from macroscopic anisotropy.

friction coefficient μ between grains, for the loading regime in the interval D–A shown in Fig. 1. The relation between anisotropy and friction is linear to a very good approximation in the range $0.1<\mu<0.3$, where it is particularly simple. This is also a realistic interval of the frictional parameter, applicable to an ample set of materials. It is clear that one cannot extend such a fit to lower values of the local friction as it becomes nonlinear as the limit of zero local friction corresponds to a small global anisotropy. The latter limit is interesting and should be addressed further since confinement and geometry can yield an apparent macroscopic friction [21].

The linear range in Fig. 5 lends itself to the following relation derived from the definition of anisotropy:

$$\frac{\sigma_3}{\sigma_1} = \frac{1}{1-\alpha\mu-\delta}, \tag{4}$$

where $\alpha=1.1$ and $\delta=0.37$ are both dimensionless parameters from Fig. 5 and the ratio σ_3/σ_1 is a constant for a fixed μ, where the anisotropy has saturated (see inset of Fig. 1). We take $\sigma_1\sim\sigma_2$ from symmetry and actual computations. If the line drawn from the tangents of the loading Mohr circles in Fig. 4 is assumed to be the Coulomb failure criterion line, $\tau=\mu_M\sigma$ (for cohesionless material) then $\tan\phi=\mu_M$ as shown in the figure. On the other hand, the relation $\sigma_3/\sigma_1=(1+\sin\phi)/(1-\sin\phi)$ follows from the Coulomb criterion [22]. From Fig. 4, $\phi\sim\pi/6$, so that the macroscopic friction coefficient implied is $\mu_M\sim 1/\sqrt{3}\sim 0.577$. This is also, in principle, the friction coefficient that generates the observed angle of repose for the same granular material [22].

Note that this macroscopic friction coefficient is larger than the microscopic one, set here at $\mu=0.3$ for grain-grain interactions. This fact is expected since the granular detail of the sheared planes of the material is a structural factor that has not been taken into account in the Coloumb criterion. Such an effect should require an additional apparent frictional effect, lumped into the macroscopic friction coefficient μ_M. While the angle of internal friction implied by the macroscopic friction coefficient has a clear meaning in rock failure, its meaning in cohesionless granular has been established in Ref. [23] only for a very particular boundary condition, where slip planes can develop. This is not the case for either fixed wall or periodic boundary conditions studied here. The latter case has been analyzed in two dimensions experimentally in Ref. [24], where a connection is also made between the microscopic friction and macroscopic friction from Rankine analysis. Their results also demonstrate a greater macroscopic friction due to structural effects, on the basis of simple geometrical models assuming a peaked distribution of particle radii. A related study of the geometrical effects on macroscopic friction is that of Ref. [25] where, as in [24], a local friction angle can be defined by the ratio of the local tangential and normal forces.

The unloading process is starkly different: here the Young modulus is by no means constant and the failure criterion cannot be globally Coulombic because it is implied that σ_3 should be proportional to $1/2(\sigma_1+\sigma_2)$. For unloading, if we believe only in a local Coulomb criterion [3], we can think that, as the granular pile fails, the effective friction coefficient changes. Using again the Coulomb-Mohr construction where local tangents are taken from a curve joining succesive Mohr circles during unloading, we can define an internal friction angle, where a sort of reverse failure first occurs, at a very high $\mu_M\sim 1.73$. This is consistent with the fact that the pile is unloaded and nevertheless it barely changes its lateral stress (see Fig. 1). Then the pile fails significantly and the effective friction decreases abruptly to $\mu_M=0.6$, and gradually progresses to zero, i.e., the pile is effectively frictionless, as we approach the hydrostatic and stress anisotropy switching point. Here, the geometry of the pack somehow acts to reduce the macroscopic friction. Finally, below the hydrostatic point, we have an inverted Mohr circle ($\sigma_3<\sigma_1$) with very small effective frictions. This corresponds to the switched configuration where the strong network is transverse to the remaining uniaxial stress.

The previous results suggest that there is an interplay between geometry and the microscopic friction to give an effective macroscopic friction. This relation depends in detail on the fabric structure of the network, especially for the unloading regime. Two-dimensional models can give us insight into the relation between the fabric and the macroscopic behavior of the pile. In Ref. [24], the author relates the normal and tangential forces applied to a plane in the material (macroscopic description) to the normal and tangential forces between grains composing that plane. Once microscopic friction is set, one only has one parameter to determine, which depends on the range of angles that the fabric between two grains can take on a particular plane. Such ranges are not clear without the fabric information incorporated in a more formal model in Ref. [25]. Applications to three dimensions seem more involved and need separate attention.

V. CONCLUSIONS

Summarizing, we have addressed hysteresis and anisotropy of a three-dimensional granular pack under uniaxial stress, from both microscopic and macroscopic point of view. We found that separation between a strong network and a weak network makes sense, and that these networks behave in a very distinguishable fashion in terms of their anisotropy as a function of loading and unloading. Fabric anisotropy during the first steps of loading exhibits signatures of arching or total transmission of uniaxial stress toward the lateral dimensions. At higher loadings, the strong network assumes a positive anisotropy while the weak network is mainly directed laterally.

Unloading is very different, and begins with large changes in the weak network accompanied by a virtual paralysis of the strong network. Further unloading takes the granular pack through a fabric-wide hydrostatic point where both networks essentially point equally in every direction. At this point, the macroscopic anisotropy is also zero. Finally, the roles of the strong and weak networks switch, the strong network pointing in the lateral direction while the weak has positive anisotropy. These fabric anisotropies remain when the load is completely lifted, and defines what is known in soil mechanics as the overconsolidated state.

Mohr's circle is introduced to illustrate the behavior of the main stresses and the macroscopic shear and normal stresses on every plane. The circle serves to define a macroscopic internal friction angle that is very simply related to the microscopic, grain-grain friction. During loading, an empirical relation is derived, relating anisotropy to the macroscopic friction angle. A Coulomb friction criterion producing the same global anisotropy yields in general a friction larger than the microscopic one. This can be justified in terms of two-dimensional models where the geometry of the strained planes tends to increase the effective friction. On unloading, the picture is much less clear, and only a local Coulomb model is proposed to interpret the continuously changing effective friction. The switching point, addressed following the fabric results, corresponds to a zero effective friction situation, while for the final stages of unloading the effective friction is very low or not well-defined at all.

The interplay between microscopic friction and the geometry of the fabric needs to be studied further, probably in two dimensions, in order to simplify the models. Preliminary assessments in this direction, based on Ref. [24], show that geometry can indeed yield both higher and lower friction angles as compared to the microscopic ones. Proper treatments should nevertheless include fabric information in order to include orientation effects of the forces. Work in this direction is in progress.

ACKNOWLEDGMENTS

Discussions with Carlos Santos are gratefully acknowledged. This work was supported by the IVIC Rocks project and by POLAR Enterprises through a LOCTI grant.

[1] J. Duran, *Sands, Powders, and Grains* (Springer, Berlin, 2000).
[2] D. L. Johnson *et al.*, ASME J. Appl. Mech. **65**, 380 (1998).
[3] J. C. Jaeger, N. G. W. Cook, and R. W. Zimmerman, *Fundamentals of Rock Mechanics*, 4th ed. (Blackwell, London, 2007).
[4] I. Agnolin and J. N. Roux, Phys. Rev. E **76**, 061302 (2007); **76**, 061303 (2007); **76**, 061304 (2007).
[5] H. A. Makse, N. Gland, D. L. Johnson, and L. M. Schwartz, Phys. Rev. Lett. **83**, 5070 (1999).
[6] F. Radjai, D. E. Wolf, M. Jean, and J. J. Moreau, Phys. Rev. Lett. **80**, 61 (1998); F. Radjai, M. Jean, J. J. Moreau, and S. Roux, *ibid.* **77**, 274 (1996).
[7] L. E. Silbert, G. S. Grest, and J. W. Landry, Phys. Rev. E **66**, 061303 (2002).
[8] X. Zeng and N. Bi, J. Geotech. Geoenviron. Eng. **125**, 741 (1999).
[9] S. Vega, Ph.D. thesis, Stanford University, 2003.
[10] R. H. G. Parry, *Mohr Circles, Stress Paths and Geotechnics*, 2nd ed. (Routledge, UK, 2004).
[11] V. Sivakumar, I. G. Doran, J. Graham, and T. Navaneethan, Geotechnique **52**, 225 (2001).
[12] X. García and E. Medina, Geophysics **71**, 13 (2006).
[13] F. Preisach, Z. Phys. **94**, 277 (1935); I. D. Mayergoyz, J. Appl. Phys. **57**, 3803 (1985).
[14] R. A. Guyer, K. R. McCall, and G. N. Boitnott, Phys. Rev. Lett. **74**, 3491 (1995).
[15] D. M. Mueth, H. M. Jaeger, and S. R. Nagel, Phys. Rev. E **57**, 3164 (1998); G. Lovoll, K. J. Maloy, and E. G. Flekkoy, *ibid.* **60**, 5872 (1999).
[16] T. S. Majmudar and R. P. Behringer, Nature (London) **435**, 1079 (2005).
[17] J. Schafer, S. Dippel, and D. E. Wolf, J. Phys. I **6**, 5 (1996).
[18] X. García, M. Araujo, and E. Medina, Waves Random Media **14**, 129 (2004).
[19] T. Bourbie, O. Coussy, and B. Zinszner, *Acoustics of Porous Media* (Gulf, Houston, 1987).
[20] M. Madadi, O. Tsoungui, M. Latzel, and S. Luding, Int. J. Solids Struct. **41**, 2562 (2004).
[21] S. Luding, J. Phys.: Condens. Matter **17**, S2623 (2005).
[22] R. M. Nedderman, *Statics and Kinematics of Granular Materials* (Cambridge University Press, Cambridge, UK, 2005).
[23] J. A. Astrom, H. J. Herrmann, and J. Timonen, Phys. Rev. Lett. **84**, 638 (2000).
[24] W. Eber, Phys. Rev. E **69**, 021303 (2004).
[25] B. Cambou, Ph. Dubujet, and C. Nouguier-Lehon, Mech. Mater. **36**, 1185 (2004).